

# Distributed Control for State of Charge Balancing Between the Modules of a Reconfigurable Battery Energy Storage System

Thomas Morstyn, *Student Member, IEEE*, Milad Momayyezani, *Student Member, IEEE*,  
Branislav Hredzak, *Senior Member, IEEE*, and Vassilios G. Agelidis, *Fellow, IEEE*

**Abstract**—This paper presents a distributed control strategy for state of charge balancing between the battery modules of a reconfigurable battery energy storage system. The autonomous modules share state of charge information with their neighbours over a sparse communication network and cooperate to reach a balanced state of charge. The proposed control strategy provides advantages in terms of reduced communication requirements, and increased modularity, over a centralised battery management system. Steady state analysis provides bounds on the mean error and mean squared error of the distributed average state of charge estimates used for autonomous balancing control. The proposed control strategy enforces module topology constraints specific to the particular reconfigurable battery implementation. The state of charge balancing mode current controller prevents current spikes during module topology transitions. Experimental results demonstrate the performance of the proposed control strategy for a reconfigurable energy storage system made up of four 6V, 7Ah lead-acid battery modules.

**Index Terms**—Reconfigurable battery, state of charge estimation, state of charge balancing, distributed cooperative control, dynamic average consensus.

## I. INTRODUCTION

**B**ATTERY energy storage (ES) technologies offer a wide range of power and energy densities, making them suitable for both mobile applications and fixed bulk storage applications [1]. Demand for battery ES is being driven by increasing interest in electric vehicles and power network storage, as well as reductions in the cost of battery technologies [2], [3].

Individual battery cells have low voltage and low current capacity. To overcome this, most battery ES systems have multiple modules connected in series and parallel, with each module made up of multiple series connected cells [4]. Generally, a DC–DC converter is used to provide a controllable power interface between the battery modules and the load [5]. However, individual modules are expected to have different properties and operating conditions, so that even when the modules are operated with the same current, their states of charge (SoC) may diverge [6]. If any of the modules in a series connected string empty, the entire string will be unable to provide energy. Conversely, if one of the modules becomes

full, the string should not be charged further [7]. This reduces the effective capacity of the battery ES system. Therefore, to fully utilise the capacity of a battery ES system, a module balancing strategy is required.

Battery module SoC balancing can be provided by introducing an additional balancing circuit between the modules [8]. Another approach is to use individually controlled DC–DC converters for each battery module [9]. However, both of these approaches require a significant number of additional components.

Reconfigurable battery ES systems have been proposed for a range of applications [10]–[13]. Reconfigurable battery ES systems incorporate a module switching circuit allowing the topology of the battery modules connected to the DC–DC converter to be controlled. This allows a single power converter to be used for a range of functions, including charging, load feeding and SoC balancing. The voltage and current capacity of the reconfigurable ES system can be adjusted by changing the number of modules connected in series and parallel, increasing its flexibility and operating range. Also, adding redundant modules can provide additional robustness.

Centralised SoC balancing control strategies have been presented for ES systems with reconfigurable battery modules [11], [12] and modules with individual converters [9], [14]. However, for a large battery ES system made up of many modules, expensive processing and communications infrastructure will be required to support centralised SoC estimation and control.

Distributed battery module monitoring has been proposed to deal with these issues, with modules connected by a sparse communication network to a central controller [15], [16]. Building on this trend, a distributed control strategy can be achieved by moving autonomous control functions to distributed hardware located at each battery module. Under a distributed control strategy, autonomous agents use neighbour to neighbour communication over a sparse communication network to cooperate and achieve common objectives [17].

Distributed control provides advantages in terms of reduced communication requirements, and increased modularity [18]. For the future smart grid, distributed control could also have security advantages, allowing coordination between networked storage systems without data centralisation, which could lead to intellectual property and privacy concerns [19], [20]. Distributed control has been used in AC and DC microgrids for secondary control [21]–[23] and SoC balancing between

T. Morstyn, M. Momayyezani, B. Hredzak and V. G. Agelidis are with the Australian Energy Research Institute and the School of Electrical Engineering and Telecommunications, University of New South Wales (UNSW Australia), Sydney, NSW 2052 Australia (email: t.morstyn@student.unsw.edu.au, m.momayyezani@student.unsw.edu.au, b.hredzak@unsw.edu.au, vassilios.agelidis@unsw.edu.au).

distributed battery ES systems [24]–[30]. Distributed control has also been used to coordinate load sharing between parallel DC–DC converters [31], [32]. A distributed control strategy for voltage balancing between reconfigurable battery cells is presented in [33]. However, battery SoC dynamics are not considered. Battery voltage is only a good indication of SoC when the battery current is very low, and after a significant charge recovery period. This limits the speed a voltage balancing control strategy can provide accurate SoC balancing. Also, the reconfigurable ES system considered in the paper allows any series connected module to be included or excluded from the string of modules supplying the load, and it is assumed that module topology constraints do not need to be enforced.

This paper presents a distributed control strategy for SoC balancing between the battery modules of a reconfigurable battery ES system. Each module has a distributed battery management system (DBMS) that performs the current and voltage monitoring and processing required for SoC estimation. The DBMSs operate autonomously, communicating with their neighbours over a sparse communication network to cooperate and achieve SoC balancing. This reduces the communication and processing infrastructure compared to a centralised battery management system implementation. Battery modules added to the reconfigurable ES system can be included in the SoC balancing strategy by connecting new DBMSs to the communication network, improving scalability. A module switching circuit logic block enforces constraints on the module topology specific to the particular reconfigurable battery implementation. This decouples the higher level distributed SoC estimation and cooperative control from the module switching circuit implementation, providing modularity and allowing the control strategy to be used for different reconfigurable battery ES systems. Steady state analysis provides bounds on the mean error and mean squared error of the distributed average SoC estimates used for autonomous balancing control. In this paper the proposed control strategy is demonstrated for the reconfigurable battery ES system from [13]. This battery ES system achieves low switch count by imposing restrictions on the possible module configurations. A SoC balancing current control is implemented that prevents current spikes during module topology transitions. Experimental results demonstrate the performance of the proposed control strategy for a reconfigurable ES system with four 6V, 7Ah lead-acid modules.

This paper is organised as follows. Section II describes the principle of operation for the proposed control strategy. Section III presents the module switching logic for a low switch count reconfigurable battery ES system. Section IV presents the distributed SoC estimation strategy. Experimental results demonstrating the performance of the proposed control strategy are provided in Section V. Section VI concludes the paper.

## II. PRINCIPLE OF OPERATION

Fig. 1 shows a high level block diagram for a reconfigurable battery ES system with the proposed distributed SoC balancing control strategy.

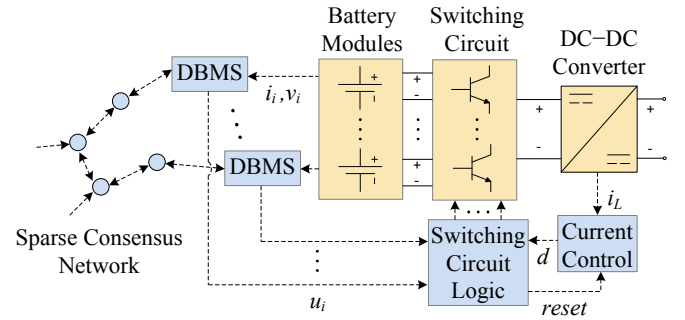


Fig. 1. High level block diagram for a reconfigurable battery ES system with the proposed battery module SoC balancing control strategy.

The main physical components of a reconfigurable battery ES system are a matrix of battery modules, a module switching circuit, and a DC–DC converter that provides a controllable power interface between the battery modules and the load [12], [13]. The control strategy is made up of a distributed battery management system (DBMS) at each module, with local SoC monitoring and control functions, a sparse communication network allowing neighbour to neighbour communication between the DBMSs, a balancing mode current controller, and a switching circuit logic block that controls the module switching circuit based on the control signals from the DBMSs.

The objective of the proposed control strategy is to control the transfer of energy between the reconfigurable battery ES system modules so that they achieve a balanced SoC.

### A. Distributed Battery Management Systems

Each module's DBMS measures the local voltage and current, and uses a Kalman filter to update a local module SoC estimate. The DBMSs share their local SoC estimates with their neighbours over a sparse communication network, and update local estimates of the average module SoC according to a dynamic average consensus protocol. The structure of the dynamic average consensus protocol ensures that in steady state, the average SoC estimates will have bounded mean error and mean squared error, as shown in Section IV. The dynamic average consensus protocol requires only a symmetric communication network with a spanning tree between the modules. The communication network topology doesn't need to match the physical connections between the battery modules.

### B. Module Switching Circuit Logic

Each DBMS generates a binary control signal, which is HIGH if the local SoC estimate is above the local estimate of the average module SoC, and LOW otherwise. These control signals are updated at the sampling interval of the DBMS Kalman filters, and are sent to the switching circuit logic block. Based on these control signals, the switching circuit logic block sets the gate signals of the module switching circuit to achieve SoC balancing.

The switching circuit logic block is the only component of the proposed control strategy that depends on the physical

realisation of the module switching circuit. The switching circuit logic will be fully distributed if each module has dedicated switches allowing it to be connected or excluded from the string supplying the DC–DC converter. An example of this type of reconfigurable battery ES system topology is found in [12]. For this type of topology, when feeding a load, each module with high SoC would control its local switches to join the string supplying the converter. Conversely, during charging, each module with low SoC would join the string.

Where there are restrictions on the possible module connection topologies, such as in [13], the switching circuit logic will have module interdependencies, and will no longer be fully distributed. However, the switching circuit logic block requires minimal processing and communications infrastructure compared to the distributed SoC and average SoC estimation. Therefore the primary benefits of distributed control structure are maintained.

In Section III, switching circuit logic is presented for the reconfigurable battery ES system from [13] when operated in a dedicated balancing mode that utilises the DC–DC converter inductor as a storage element. The dedicated balancing mode allows for state of charge balancing between the battery modules during periods of no load. This is useful for applications such as electric vehicles, which do not require power when parked, and grid connected storage systems used for peak shaving, which may not be used during periods of moderate network load [1]. The reconfigurable battery ES system modules are swapped between a charge and discharge cycle. In the discharge cycle, modules with high SoC (above the average module SoC) are connected in forward bias with the inductor, which stores energy. In the charge cycle, all of the modules are connected in reverse bias with the inductor, and are thus charged. Proper selection of the modules included in the discharge cycle provides SoC balancing.

### C. Current Control

During the discharge cycle, the inductor current increases, as energy is stored in the inductor. During the charge cycle it decreases, as energy is transferred back to the battery modules. A PI current controller sets the duty cycle of the discharge cycle to regulate the inductor current to a desired reference. When a module transition occurs, the inductor voltage changes suddenly and a significantly different duty cycle may be required to achieve the same inductor current. To prevent a transient spike in the battery current, the PI controller is reset by a signal from the switching circuit logic block, and an additional long charge cycle is introduced. This transfers the energy stored in the inductor to the battery modules, before the new voltage is applied. The current control does not require information from the individual battery modules.

## III. BATTERY MODULE SWITCHING CIRCUIT LOGIC

The switching circuit logic is specific to the particular reconfigurable battery implementation and operating mode. In this section, switching circuit logic is presented for the reconfigurable battery ES system from [13] when operated in a dedicated balancing mode that utilises the DC–DC converter

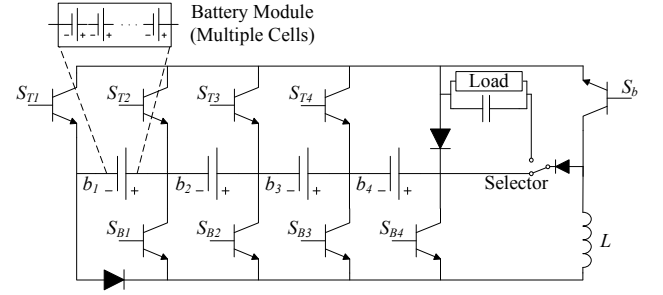


Fig. 2. Low switch count reconfigurable battery ES system with four modules.

inductor as a storage element. This example demonstrates how the switching circuit logic can be designed to provide SoC balancing while also enforcing module configuration restrictions.

Fig. 2 shows the reconfigurable battery ES system topology for four modules. The module switching circuit introduces full-bridges between the modules and the supply rails of the DC–DC converter, allowing the modules to be connected in forward or reverse bias. A low switch count is achieved by having each adjacent set of modules share the full-bridge leg between them, so each additional battery module requires only two additional switches. However, this introduces restrictions on the possible module connection topologies. Also, the voltage stress on the switches is not distributed evenly. For the top and the bottom switches ( $S_{T1}$ – $S_{T4}$  and  $S_{B1}$ – $S_{B4}$ ), the stress increases from right to left and left to right respectively. Devices with different voltage ratings should be selected for each switch to optimise the cost and performance of the system.

When the selector switch is DOWN the reconfigurable battery ES system operates in a dedicated SoC balancing mode. The DC–DC converter inductor  $L$  is used as the balancing mode storage element. The module switching circuit is operated to swap between a discharging cycle, with high SoC modules in forward bias, and a charging cycle with all modules in reverse bias. The discharge and charge cycle for a four module battery ES system are shown in Fig. 3(a) and Fig. 3(b), when modules 1, 2 and 3 have high SoC.

The reconfigurable battery ES system topology in Fig. 2 allows any set of adjacent modules to be connected in forward bias with the inductor. However, the modules don't have independent bypass switches, so non-adjacent modules cannot be connected in series. For example, consider the case where energy needs to be transferred from module 1 and module 3 to the inductor. This requires  $S_{T1}$  and  $S_{B3}$  to be ON. It can be seen from Fig. 3(a) that module 2 will be included in the string supplying the inductor, regardless of whether the other switches are ON or OFF. The switching circuit logic must be designed so that SoC balancing is achieved, taking into account this restriction that only adjacent modules can be connected in series.

First, consider the case where there are only two battery modules. SoC balancing will be achieved if the module with higher SoC is connected in forward bias during the discharge cycle, and both modules are connected in reverse bias during

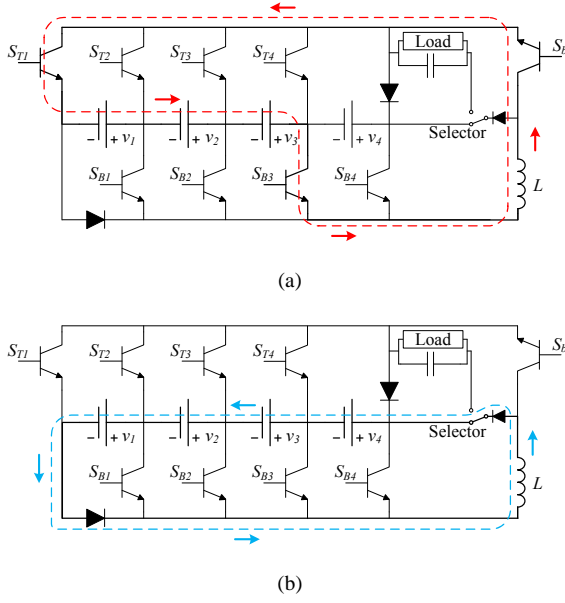


Fig. 3. Four module reconfigurable battery ES system in balancing mode, when modules 1, 2 and 3 have local SoC estimates above their average SoC estimates. (a) Discharge Cycle:  $S_{T1}$ ,  $S_{B3}$ , and  $S_b$  are ON. The current flow path is shown in red. Energy is transferred from the battery modules to the inductor. (b) Charge Cycle: All switches are off. The current flow path is shown in blue. Energy is transferred from the inductor to the battery modules.

the charge cycle. Similarly if the modules of a multi-module reconfigurable battery ES system can be divided into two blocks, with the left block modules all below the average SoC, and the right block modules all above the average SoC, then the SoC difference between all of the modules will be reduced by connecting the right block of modules in forward bias during the discharge cycle.

The switching control logic proposed for the reconfigurable battery ES system is to connect the left-most block of adjacent modules with HIGH control signals during the discharge cycle (i.e. modules that estimate their SoC is above the average module SoC). This will cause a rightward movement of charge, until all modules with high SoC are in an adjacent block on the right of the ES system. From this point, the modules in this block will be discharged, reducing the SoC difference between all of the modules.

For an  $N$  module reconfigurable battery ES system, let  $u_i$  be the binary control signal from the  $i$ th DBMS, and let  $S_{Ti}$  and  $S_{Bi}$  be the status of the  $i$ th top and bottom switch respectively. The switching control logic to achieve the desired functionality is described by the following boolean expressions.

Discharge Cycle :

$$\begin{aligned} S_{T1} &= u_1, \\ S_{Ti} &= u_i \bar{u}_{i-1} \cdots \bar{u}_1, \quad i \in \{2, \dots, N\}. \\ S_{B1} &= u_1 \bar{u}_2, \quad S_{BN} = u_N \bar{S}_{B2} \cdots \bar{S}_{BN-1}, \\ S_{Bi} &= u_i \bar{u}_{i+1} \bar{S}_{B1} \bar{S}_{B2} \cdots \bar{S}_{Bi-1}, \quad i \in \{2, \dots, N-1\}. \end{aligned}$$

Charge Cycle :

$$S_{Ti} = 0, \quad S_{Bi} = 0, \quad i \in \{1, \dots, N\}.$$

Battery modules are subject to progressive degradation as well as catastrophic failures [34]. Module failures are charac-

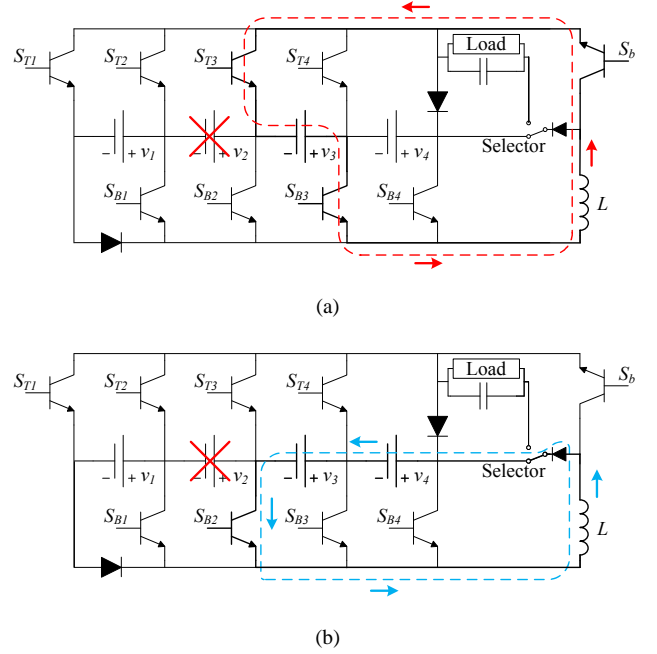


Fig. 4. Four module reconfigurable battery ES system in balancing mode. Module 2 has failed. Modules 1 and 2 are excluded from balancing. Module 3 has a local SoC estimate above the average SoC estimate. (a) Discharge Cycle:  $S_{T3}$ ,  $S_{B3}$ , and  $S_b$  are ON. The current flow path is shown in red. (b) Charge Cycle:  $S_{B2}$  is ON. The current flow path is shown in blue.

terised by an inability to provide charge, and will be detected by the DBMSs as an excessive impedance.

In the case where module failure is detected, the associated DBMS will send an error signal to the switching circuit logic block, which will modify the switching control logic to exclude the affected battery module. The restriction that non-adjacent modules cannot be connected in series means that either the modules to the left or the right of the failed module must be excluded from balancing, so the side with fewer modules is excluded. For the dynamic average consensus protocol, the DBMSs of the excluded modules will participate by simply passing on signals received from their neighbours, so that the average SoC of the non-excluded modules is calculated.

If there are fewer modules to the left of the failed module  $i$ ,  $S_{Bi}$  will be ON for the charging cycle, and  $S_{Tj}$ ,  $j \leq i$  and  $S_{Bj}$ ,  $j < i$  will be OFF for both cycles. Balancing can proceed using the switching control logic for a reconfigurable battery with modules equal to the number of modules to the right of the failed module. The discharge and charge cycle for a four module battery ES system which has had a failure in module 2 is shown in Fig. 4(a) and Fig. 4(b), when module 3 has high SoC.

If there are fewer modules to the right of the failed module  $i$ , then  $S_{Ti}$  and  $S_b$  will be ON for the charging cycle, and  $S_{Tj}$ ,  $j > i$  and  $S_{Bj}$ ,  $j \geq i$  will be OFF for both cycles. The discharge and charge cycle for a four module battery ES system which has had a failure in module 3 is shown in Fig. 5(a) and Fig. 5(b), when module 1 has high SoC.

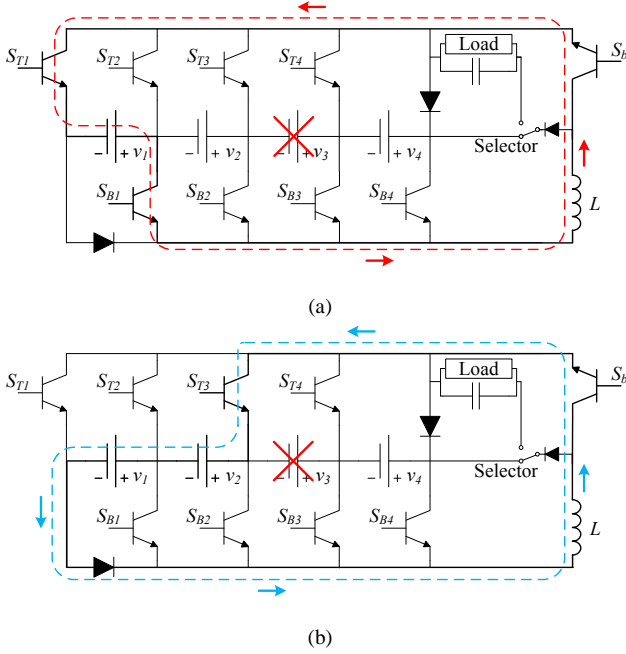


Fig. 5. Four module reconfigurable battery ES system in balancing mode. Module 3 has failed. Modules 3 and 4 are excluded from balancing. Module 1 has a local SoC estimate above the average SoC estimate. (a) Discharge Cycle:  $S_{T1}$ ,  $S_{B1}$ , and  $S_b$  are ON. The current flow path is shown in red. (b) Charge Cycle:  $S_b$  and  $S_{T3}$  are ON. The current flow path is shown in blue.

#### IV. DISTRIBUTED STATE OF CHARGE ESTIMATION

Each battery module has a DBMS with a Kalman filter to estimate the module SoC. The DBMSs also update estimates of the average SoC of the reconfigurable battery ES system modules using a dynamic average consensus protocol based on neighbour to neighbour communication over a sparse communication network.

##### A. Local Kalman Filter Based State of Charge Estimation

The battery module SoC is not directly measurable. However, it can be estimated based on output voltage and current measurements, assuming an approximate battery model is known. The second order RC circuit model shown in Fig. 6 is used to model the lead-acid battery module dynamics [35].  $C_{bi}$  and  $R_{bi}$  model the slow SoC dynamics of the battery, while  $C_{si}$  and  $R_{si}$  model the faster surface voltage dynamics.  $R_{ti}$  is the terminal resistance of the battery module.

Model uncertainty and measurement noise is modelled by introducing zero-mean white process noise  $w_i$  on the states and measurement noise  $v_i$  on the output measurements [36]. In this case a Kalman filter provides an unbiased SoC estimate with minimum error covariance. It is assumed that the process noise is uncorrelated across the ES system states, and that the process and measurement noise is uncorrelated across time and between the ES systems.

Let the  $i$ th battery module's dynamics be described by the

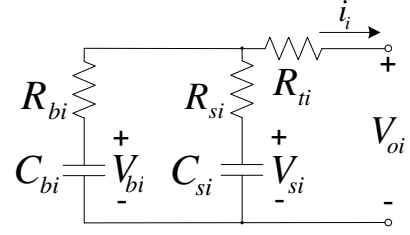


Fig. 6. Battery module circuit model.

following discrete time state space model available from [35].

$$\begin{aligned} x_i(t+h) &= A_i x_i(t) + B_i i_i(t) + w_i(t), \\ y_i(t) &= C_i x_i(t) + v_i(t) = V_{oi}(t) + v_i(t), \\ x_i(t) &= [V_{bi}(t) \ V_{si}(t) \ V_{oi}(t)]^T, \\ \mathbb{E}[w_i] &= 0, \ \mathbb{E}[v_i] = 0, \\ \mathbb{E}[w_i(t)w_i(t)^T] &= Q_i, \ \mathbb{E}[v_i(t)v_i(t)^T] = R_i. \end{aligned} \quad (1)$$

$h$  is the sampling period.

The discrete time Kalman filters are updated according to the following algorithm [37].

Prediction Step :

$$\hat{x}_i(t+h|t) = A_i \hat{x}_i(t|t) + B_i i_i(t)$$

$$P_i(t+h|t) = A_i P_i(t|t) A_i^T + Q_i$$

Update Step :

$$K(t+h) = P_i(t+h|t) C_i^T [C_i P_i(t+h|t) C_i^T + R_i]^{-1}$$

$$\tilde{y}_i(t+h) = y_i(t+h) - C_i \hat{x}_i(t+h|t)$$

$$\hat{x}_i(t+h|t+h) = \hat{x}_i(t+h|t) + K(t+h) \tilde{y}_i(t+h)$$

$$P_i(t+h|t+h) = [I - K(t+h) C_i] P_i(t+h|t).$$

At each time interval the discrete time Kalman filter provides an unbiased state estimate  $\hat{x}_i$  given by  $\hat{x}_i(t) = x_i(t) + \tilde{x}_i(t)$ , where  $x_i(t)$  is the actual module state and  $\tilde{x}_i(t)$  is the prediction error. Note that  $\mathbb{E}[\tilde{x}_i(t)] = 0$  and  $\mathbb{E}[\tilde{x}_i(t)\tilde{x}_i(t)^T] = P_i(t)$ . The steady state estimation error covariance  $\bar{P}_i$  is given by the solution to the following discrete time Riccati equation.

$$\bar{P}_i = A_i \bar{P}_i A_i^T - A_i \bar{P}_i C_i^T [C_i \bar{P}_i C_i^T + R_i]^{-1} C_i \bar{P}_i A_i^T + Q_i$$

Module SoC estimates can be obtained from the estimated bulk capacitance voltage.

$$\hat{SoC}_i = \frac{\frac{1}{2} C_b (\hat{V}_{bi}^2 - V_{b[0\%SoC]}^2)}{E_{maxi}}. \quad (2)$$

$\hat{SoC}_i$  is the estimated fraction of module energy remaining,  $V_{b[0\%SoC]}$  is the steady state open circuit voltage at 0% SoC and  $E_{maxi}$  is the rated battery capacity in Ws.

##### B. Dynamic Average Consensus

Each DBMS requires a local estimate of the average module SoC. This estimate is updated based on its local SoC estimate and information received from neighbouring modules in the sparse communication network.

Consider a reconfigurable battery ES system with  $N$  modules, each with a DBMS. The communication network between them is described by a graph  $\mathcal{G}(\mathcal{V}, \mathcal{E})$ , where  $\mathcal{V} = \{1, \dots, N\}$  are nodes, each representing a DBMS, and  $(i, j) \in \mathcal{E}$  is an edge, representing a communication link allowing information to flow from node  $i$  to node  $j$ . The neighbours of node  $i$  are given by  $j \in \mathcal{N}_i$ , where  $(j, i) \in \mathcal{E}$ . Each communication link has a link weight  $a_{ij}$ . The graph dynamics are described by a consensus matrix  $\mathbf{A}$ .

$$[\mathbf{A}]_{ij} = \begin{cases} 1 - \sum_{j \in \mathcal{N}_i} a_{ij}, & i = j \\ a_{ij}, & i \neq j \\ 0, & \text{otherwise.} \end{cases} \quad (3)$$

In [38], the following first order dynamic average consensus protocol, with update period  $h$ , is introduced.

$$x_{ri}(t+h) = x_{ri}(t) + \sum_{j \in \mathcal{N}_i} a_{ij}(x_{rj}(t) - x_{ri}(t)) + \Delta r_i(t). \quad (4)$$

$r_i(t)$  is the reference signal at node  $i$  and  $x_{ri}(t)$  is node  $i$ 's estimate of the average reference.  $\Delta$  is the difference operator, so  $\Delta r_i(t) = r_i(t) - r_i(t-h)$ . The global consensus dynamics are given by

$$\begin{aligned} \mathbf{x}_r(t+h) &= \mathbf{A}\mathbf{x}_r(t) + \Delta \mathbf{r}(t), \text{ where} \\ \mathbf{x}_r &= [x_{r1} \dots x_{rN}]^T, \Delta \mathbf{r} = [\Delta r_1 \dots \Delta r_N]^T. \end{aligned} \quad (5)$$

Let the communication link weights be chosen so that the communication network is symmetric ( $\mathbf{A} = \mathbf{A}^T$ ), and there exists  $\alpha > 0$  such that the following average consensus conditions are satisfied [39].

- 1)  $a_{ii} \geq \alpha, \forall i$ .
- 2)  $a_{ij} \in \{0\} \cup [\alpha, 1], \forall i, j$ .
- 3)  $\mathbf{A}\mathbf{1} = \mathbf{1}$ .

Under these conditions the following conservation property holds [38].

$$\mathbf{1}^T \mathbf{x}_r(t+h) = \mathbf{1}^T \mathbf{r}(t). \quad (6)$$

If the reference signals have bounded first order differences,  $\Delta r_i(t) < \infty, \forall t$ , and the communication network provides a path between all of the nodes, then the estimates of the reference average will have bounded steady state error,  $\lim_{t \rightarrow \infty} x_{ri}(t) - \frac{1}{N} \mathbf{1}^T \mathbf{r}(t) < \infty$  [38]. The convergence rate of discrete time consensus algorithms is analysed in [39]. The convergence rate can be increased by reducing the update period and providing additional communication links.

The objective for the DBMSs is to reach consensus at the average of the local SoC estimates. Therefore, each DBMS sets its consensus protocol reference  $r_i(t)$  equal to its local SoC estimate (2). However, although the state estimates from the local Kalman filters have bounded steady state covariance, they do not have bounded first order differences.

The distributed average consensus protocol (4) has unbounded steady state error for references with unbounded first order differences. Despite this, the following section shows that meaningful consensus is still provided, since the average state estimates have bounded steady state mean squared error. This is due to the difference operator applied to the reference signals, which prevents the SoC estimation error from com-

pounding over time.

### C. Steady State Analysis

The dynamic average consensus steady state mean error and mean squared error provide statistical measures of the estimation accuracy. The estimation accuracy limits the accuracy of the SoC balancing control strategy, since the energy transfers between the modules are decided by their estimates of the average module SoC.

The dynamic average consensus protocol error is given by,

$$\tilde{\mathbf{x}}_r(t+h) = \mathbf{x}_r(t+h) - \frac{\mathbf{1}\mathbf{1}^T}{N} \mathbf{r}(t). \quad (7)$$

Let the matrix  $P = (I - \frac{\mathbf{1}\mathbf{1}^T}{N})$ , where the elements of  $P\mathbf{x}$  are the differences between the elements of  $\mathbf{x}$  and their average. From the conservation property (6),

$$\tilde{\mathbf{x}}_r(t+h) = P\mathbf{x}_r(t+h). \quad (8)$$

Assuming there is a path between the DBMSs and the average consensus conditions are satisfied,  $\mathbf{A}$  has a single eigenvalue with magnitude 1, and all other eigenvalues strictly inside the unit circle [39]. In this case  $P$  has the following properties,  $P\mathbf{A} = \mathbf{A}P$ ,  $P = P^2$  and all eigenvalues of  $P\mathbf{A}P$  are strictly inside the unit circle [40].

The total mean squared error is given by

$$\text{MSE}_{\text{total}} = \text{trace}(\mathbb{E}[\tilde{\mathbf{x}}_r(t+h)\tilde{\mathbf{x}}_r(t+h)^T]). \quad (9)$$

Using (5),

$$\begin{aligned} &\mathbb{E}[\tilde{\mathbf{x}}_r(t+h)\tilde{\mathbf{x}}_r(t+h)^T] \\ &= \mathbb{E}[(P\mathbf{A}\mathbf{x}_r(t) + P\Delta \mathbf{r}(t))(P\mathbf{A}\mathbf{x}_r(t) + P\Delta \mathbf{r}(t))^T] \\ &= P\mathbf{A}\mathbb{E}[\tilde{\mathbf{x}}_r(t)\tilde{\mathbf{x}}_r(t)^T]\mathbf{A}P + P\mathbf{Q}P, \end{aligned} \quad (10)$$

where,  $\mathbf{Q} = \mathbf{A}\mathbb{E}[\tilde{\mathbf{x}}_r(t)\Delta \mathbf{r}(t)^T] + \mathbb{E}[\Delta \mathbf{r}(t)\tilde{\mathbf{x}}_r(t)^T]\mathbf{A} + \mathbb{E}[\Delta \mathbf{r}(t)\Delta \mathbf{r}(t)^T]$ .

The vector of local SoC estimates  $\mathbf{r}(t)$  can be expressed as,

$$\mathbf{r}(t) = \bar{\mathbf{r}}(t) + \tilde{\mathbf{r}}(t), \quad (11)$$

where  $\bar{\mathbf{r}}(t)$  is the actual SoC vector and  $\tilde{\mathbf{r}}(t)$  is a vector of SoC estimation errors, with bounded steady state mean  $\lim_{t \rightarrow \infty} \mathbb{E}[\tilde{\mathbf{r}}(t)] = \mathbb{E}[\tilde{\mathbf{r}}]_{ss}$  and covariance  $\lim_{t \rightarrow \infty} \mathbb{E}[\tilde{\mathbf{r}}(t)\tilde{\mathbf{r}}(t)^T] - \mathbb{E}[\tilde{\mathbf{r}}(t)]\mathbb{E}[\tilde{\mathbf{r}}(t)]^T = \Sigma_{\tilde{\mathbf{r}}}$ .

The dynamic average consensus protocol mean error is given by

$$\begin{aligned} \mathbb{E}[\tilde{\mathbf{x}}_r(t+h)] &= P\mathbf{A}\mathbb{E}[\mathbf{x}_r(t)] + P\mathbb{E}[\Delta \mathbf{r}(t)] \\ &= P\mathbf{A}\mathbb{E}[\mathbf{x}_r(t)] + P(\Delta \bar{\mathbf{r}}(t) + \mathbb{E}[\Delta \tilde{\mathbf{r}}(t)]). \end{aligned} \quad (12)$$

In steady state, let the change in the battery module SoC each sampling period be given by  $\Delta \bar{\mathbf{r}}_{ss}$ . In this case the steady state mean error is given by,

$$\lim_{t \rightarrow \infty} \mathbb{E}[\tilde{\mathbf{x}}_r(t)] = \mathbb{E}[\tilde{\mathbf{x}}_r]_{ss} = [I - P\mathbf{A}]^{-1} P\Delta \bar{\mathbf{r}}_{ss}. \quad (13)$$



Next, the steady state terms of  $\mathbf{Q}$  will be obtained.

$$\begin{aligned} & \mathbb{E}[\tilde{\mathbf{x}}_r(t)\Delta\mathbf{r}(t)^T] \\ &= P\mathbb{E}[(\mathbf{A}\tilde{\mathbf{x}}_r(t-h) + \Delta\mathbf{r}(t-h))\Delta\mathbf{r}(t)^T] \\ &= P\mathbf{A}\mathbb{E}[\tilde{\mathbf{x}}_r(t-h)](\Delta\bar{\mathbf{r}}(t) + \mathbb{E}[\Delta\tilde{\mathbf{r}}(t)])^T \\ & \quad + P(\Delta\bar{\mathbf{r}}(t-h)\Delta\bar{\mathbf{r}}(t)^T + \mathbb{E}[\Delta\tilde{\mathbf{r}}(t-h)]\Delta\bar{\mathbf{r}}(t)^T \\ & \quad + \Delta\bar{\mathbf{r}}(t-h)\mathbb{E}[\Delta\tilde{\mathbf{r}}(t)^T] + \mathbb{E}[\Delta\tilde{\mathbf{r}}(t-h)]\Delta\bar{\mathbf{r}}(t)^T). \end{aligned} \quad (14)$$

Therefore,

$$\lim_{t \rightarrow \infty} \mathbb{E}[\tilde{\mathbf{x}}_r\Delta\mathbf{r}^T] = P(\mathbf{A}\mathbb{E}[\tilde{\mathbf{x}}_r]_{ss}\Delta\bar{\mathbf{r}}_{ss}^T + \Delta\bar{\mathbf{r}}_{ss}\Delta\bar{\mathbf{r}}_{ss}^T - \Sigma_{\tilde{\mathbf{r}}}). \quad (15)$$

Similarly,

$$\lim_{t \rightarrow \infty} \mathbb{E}[\Delta\mathbf{r}\tilde{\mathbf{x}}_r^T] = (\Delta\bar{\mathbf{r}}_{ss}\mathbb{E}[\tilde{\mathbf{x}}_r]_{ss}^T\mathbf{A} + \Delta\bar{\mathbf{r}}_{ss}\Delta\bar{\mathbf{r}}_{ss}^T - \Sigma_{\tilde{\mathbf{r}}})P. \quad (16)$$

Finally,

$$\begin{aligned} \mathbb{E}[\Delta\mathbf{r}(t)\Delta\mathbf{r}(t)^T] &= \Delta\bar{\mathbf{r}}(t)\Delta\bar{\mathbf{r}}(t)^T + \mathbb{E}[\Delta\tilde{\mathbf{r}}(t)]\Delta\bar{\mathbf{r}}(t)^T \\ & \quad + \Delta\bar{\mathbf{r}}(t)\mathbb{E}[\Delta\tilde{\mathbf{r}}(t)^T] + \mathbb{E}[\Delta\tilde{\mathbf{r}}(t)\Delta\tilde{\mathbf{r}}(t)^T]. \end{aligned} \quad (17)$$

Therefore,

$$\lim_{t \rightarrow \infty} \mathbb{E}[\Delta\mathbf{r}\Delta\mathbf{r}^T] = \Delta\bar{\mathbf{r}}_{ss}\Delta\bar{\mathbf{r}}_{ss}^T + 2\Sigma_{\tilde{\mathbf{r}}}. \quad (18)$$

The steady state solution  $\lim_{t \rightarrow \infty} P\mathbf{Q}P = P\mathbf{Q}_{ss}P < \infty$  can be obtained from (15), (16) and (18). Since the eigenvalues of  $P\mathbf{A}P$  are strictly inside the unit circle, and  $P\mathbf{Q}_{ss}P < \infty$ , the steady state total mean squared error is bounded,  $\text{MSE}_{\text{totalss}} = \text{trace}(\mathbb{E}[\tilde{\mathbf{x}}_r\tilde{\mathbf{x}}_r^T]_{ss})$ .  $\mathbb{E}[\tilde{\mathbf{x}}_r\tilde{\mathbf{x}}_r^T]_{ss}$  can be obtained by solving the following Lyapunov equation.

$$\mathbb{E}[\tilde{\mathbf{x}}_r\tilde{\mathbf{x}}_r^T]_{ss} = P\mathbf{A}\mathbb{E}[\tilde{\mathbf{x}}_r\tilde{\mathbf{x}}_r^T]_{ss}\mathbf{A}P + P\mathbf{Q}_{ss}P. \quad (19)$$

Since the communication network is symmetric, the average consensus conditions will be maintained even in the case of communication link failure. Therefore, as long as the communication network still provides a path between the DBMSs in steady state, the DBMSs will obtain estimates of the average module SoC with bounded mean error and mean squared error. Redundant links above those required to provide a path between the DBMSs will improve the tolerance of the network to communication link failure.

## V. EXPERIMENTAL RESULTS

Experimental results demonstrate the performance of the proposed distributed SoC balancing control strategy. For safety considerations, the control strategy was tested on a low voltage reconfigurable battery ES system prototype with four 6V, 7Ah lead-acid modules. A full sized system would be in range of hundreds of volts for practical applications such as DC microgrids or electric vehicles. In [13] a reconfigurable ES system with three 132V modules, each made up of 11 series 12V 180 Ah lead acid cells, is evaluated.

The parameters of the reconfigurable battery ES system are listed in Table I. The battery module parameters were obtained using the system identification procedure from [35].

The distributed control strategy was implemented virtually on a dSPACE DS1006 Processor Board. The sampling period

TABLE I  
RECONFIGURABLE BATTERY ES SYSTEM PARAMETERS

DC-DC Converter and Control System					
Inductor	1.02mH	$f_s$	20kHz	$k_p$	0.05
$k_i$	0.2	$T_s^{KF}$	100ms	$T_s^{avg}$	100ms
Lead-Acid Battery Modules					
$V_{b[100\%SoC]}$	6V	$E_{max}$	42Wh	$R_t$	97.6m $\Omega$
$V_{b[0\%SoC]}$	5.4V	$R_b$	32.5m $\Omega$	$R_s$	32.5m $\Omega$
$C_b$	44211F	$C_s$	23.23F	$R$	0.037
$Q^{V_b}$	$1 \times 10^{-7}$	$Q^{V_s}$	$1 \times 10^{-6}$	$Q^{V_o}$	$1 \times 10^{-5}$

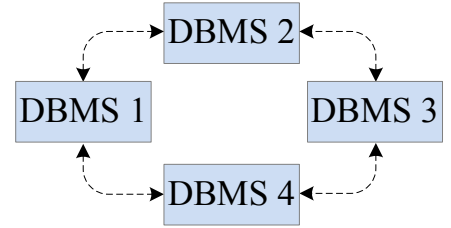


Fig. 7. The sparse communication network topology connecting the DBMSs.

of the local Kalman filters  $T_s^{KF}$  and the dynamic average consensus protocol updated period  $T_s^{avg}$  were set to 100ms. The topology of the sparse communication network connecting the DBMSs is shown in Fig. 7.

A 1A inductor current reference was selected. The small signal transfer function between the duty cycle and inductor current is given by  $\frac{i_L(s)}{d(s)} = \frac{V_{charge} + V_{discharge}}{Ls}$ , where  $V_{discharge}$  is the combined voltage of the modules connected in forward bias with the inductor during the discharge cycle and  $V_{charge}$  is the voltage of the modules connected in reverse bias during the charge cycle [13]. The PI current controller gains were selected to be  $k_p = 0.05$  and  $k_i = 0.2$ , giving a phase margin of 89 degrees and a closed loop bandwidth between 240Hz and 333Hz, depending on the number of modules connected during the discharge cycle.

The distributed average consensus protocol steady state worst case theoretical mean error is 0.56Ws, the maximum element of  $\mathbb{E}[\tilde{\mathbf{x}}_r]_{ss}$ . This occurs when a single battery module is included in the discharge cycle, giving the maximum deviation of module SoC from the average over the update interval. The theoretical steady state total mean squared error is given by  $\text{MSE}_{\text{totalss}} = 2.10(\text{Wh})^2$ . This corresponds to an individual battery module average SoC estimate standard deviation of 0.725Wh (1.7% of the total capacity).

The battery modules begin with open circuit voltages between 5.65V and 6V, corresponding to SoC between 40% and 100%, as shown in Fig. 8. The Kalman filter estimates were initialised based on the measured output voltages of the battery modules.

The DBMSs share their SoC estimates with their neighbours every 100ms and update their local estimate of the average module SoC according to the dynamic average consensus protocol. As shown in Fig. 9, it takes approximately 1.5 seconds for the local average module SoC estimates to converge.

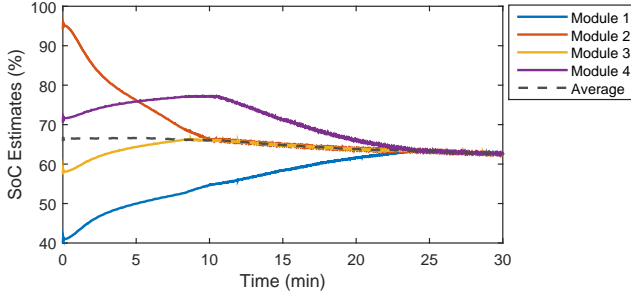


Fig. 8. Battery module SoC estimates, and the average of the SoC estimates. From 0min to 8.3min, module 2 is the left-most module with high SoC, and is the only module included in the discharge cycle. From 8.3min to 24min, combinations of modules 2, 3 and 4 are included in the discharge cycle. At 24min SoC balancing up to the estimation accuracy is achieved.

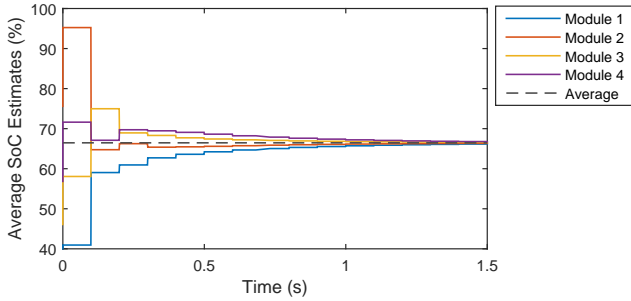


Fig. 9. Estimates of the average module SoC and the actual average shown for the first 1.5s of the distributed dynamic average consensus protocol.

Energy is transferred between the battery modules according to the module switching circuit logic described in Section III. Initially, the SoC estimates of modules 2 and 4 are above their estimate of the average SoC, and thus they have HIGH control signals. However, these modules are not adjacent and cannot be connected in series without module 3. In accordance with the module switching logic, the left-most block of adjacent modules (i.e. module 2) is connected in forward bias with the inductor during the discharge cycle, while the full string is connected in reverse bias during the charge cycle. Fig. 10(a) shows an oscilloscope screen capture with the inductor and battery module currents for several charge/discharge cycles during this period.

As shown in Fig. 8, the SoC of module 2 is reduced, while the SoC of the remaining modules increase. This continues until module 3 reaches the average SoC, after approximately 8.3 minutes. When module 3 estimates its SoC is above the average module SoC, its control signal becomes HIGH and it is included in the discharge cycle with modules 2 and 4. Fig. 10(b) shows an oscilloscope screen capture during this period. When module 3 estimates its SoC has fallen below the average, its control signal returns to LOW. This keeps module 3 near the average SoC while module 2 continues to discharge.

After 24 minutes, the SoC of all of the battery modules are approximately balanced and the SoC estimates remain within 0.4% of one another. Fig. 11 shows the battery module voltage measurements. The strong current dependence of the battery voltage demonstrates the limitations of a voltage balancing

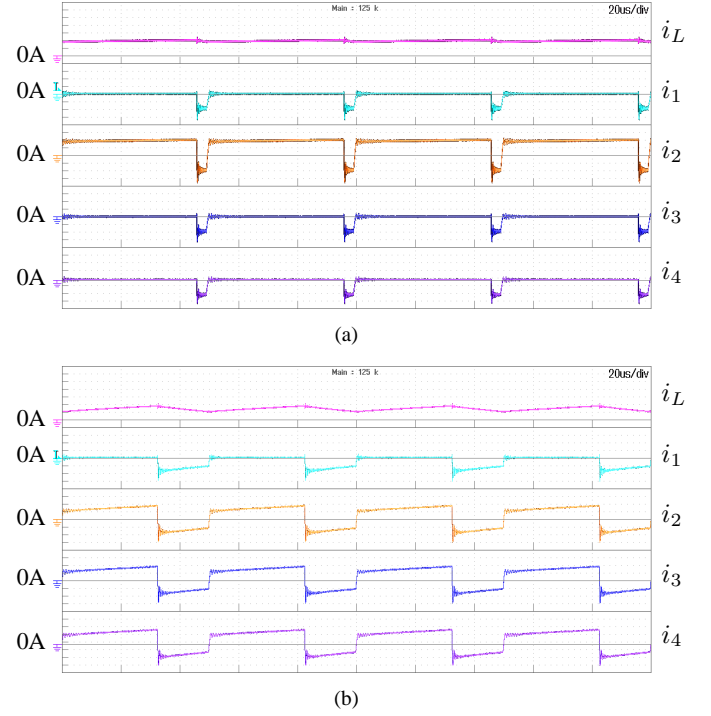


Fig. 10. Oscilloscope screen captures showing the inductor and battery module currents. X axis: 20  $\mu$ s/div, Y axis: 500mA/div. (a) Module 2 is connected in forward bias with the inductor during the discharge cycle. (b) Modules 2, 3 and 4 are connected in forward bias with the inductor during the discharge cycle.

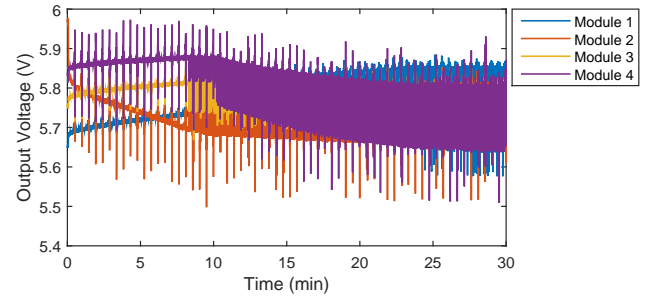


Fig. 11. Battery module voltages over the course of SoC balancing.

strategy for SoC balancing.

Fig. 12 shows the inductor current, averaged across the charge/discharge cycle, over the course of SoC balancing. The inductor current is regulated at the 1A reference, with a maximum current of 1.06A. The variations seen after 8.3min are caused by additional 20ms charge cycles inserted between module topology transitions, which reset the inductor current to zero to prevent inductor current spikes. Fig. 13 provides a zoomed in view, showing the current control performance during a module topology transition. At 501.2s, only module 2 is included in the discharge cycle. At 501.38s the control signals of modules 3 and 4 become HIGH. However, if modules 3 and 4 were suddenly included in the discharge cycle at the previous duty cycle, the inductor current would spike. To prevent this, a 20ms charge cycle is inserted so that the inductor energy is transferred to the battery modules, and the PI current controller is reset. Following the extra charge cycle,



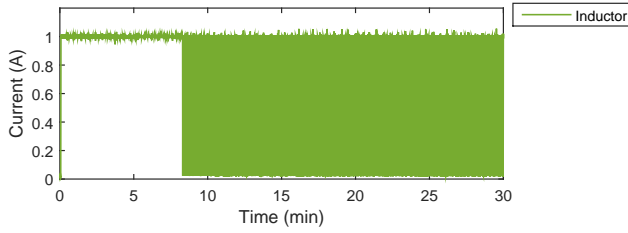


Fig. 12. Inductor current, averaged across the charge/discharge cycle, over the course of SoC balancing. The variations after 8.3min are caused by the additional 20ms charge cycles inserted between module topology transitions to prevent inductor current spikes. The maximum inductor current is 1.06A.

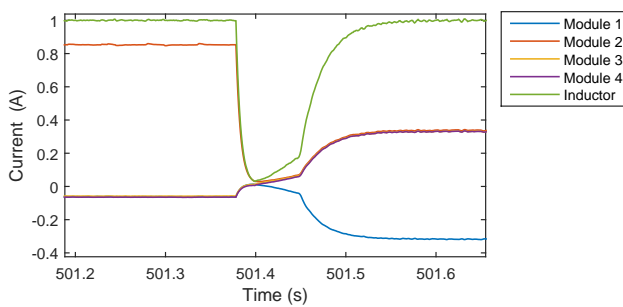


Fig. 13. Inductor and battery currents, averaged across the charge/discharge cycle, during a transition from module 2 connected in the discharge cycle, to modules 2, 3 and 4 connected in the discharge cycle. A 20ms charge cycle is inserted between the module topology transition, transferring energy from the inductor to the battery modules and preventing a spike in current.

the inductor current is regulated back to the 1A reference, without significant overshoot.

## VI. CONCLUSION

A distributed control strategy for SoC balancing between the modules of a reconfigurable battery ES system has been presented. The proposed control strategy requires only a sparse communication network between distributed battery management systems, providing advantages in terms of reduced communication requirements, and increased modularity, over a centralised battery management system. A switching circuit logic block is introduced to provide SoC balancing based on binary control signals received from the distributed battery management systems, while enforcing module topology constraints specific to the particular reconfigurable battery implementation. The performance of the proposed control strategy has been demonstrated for a reconfigurable battery ES system with four 6V, 7Ah lead-acid modules.

## REFERENCES

- [1] S. Vazquez, S. M. Lukic, E. Galvan, L. G. Franquelo, and J. M. Carrasco, "Energy Storage Systems for Transport and Grid Applications," *IEEE Transactions on Industrial Electronics*, vol. 57, no. 12, pp. 3881–3895, Dec. 2010.
- [2] H. Chen, T. N. Cong, W. Yang, C. Tan, Y. Li, and Y. Ding, "Progress in electrical energy storage system: A critical review," *Progress in Natural Science*, vol. 19, no. 3, pp. 291–312, Mar. 2009.
- [3] A. Ipekchi and F. Albuyeh, "Grid of the future," *IEEE Power and Energy Magazine*, vol. 7, no. 2, pp. 52–62, Mar. 2009.
- [4] P. Ribeiro, B. Johnson, M. Crow, A. Arsoy, and Y. Liu, "Energy storage systems for advanced power applications," *Proceedings of the IEEE*, vol. 89, no. 12, pp. 1744–1756, 2001.
- [5] N. M. L. Tan, T. Abe, and H. Akagi, "Design and Performance of a Bidirectional Isolated DC–DC Converter for a Battery Energy Storage System," *IEEE Transactions on Power Electronics*, vol. 27, no. 3, pp. 1237–1248, Mar. 2012.
- [6] C. Moo, Y. Hsieh, and I. Tsai, "Charge equalization for series-connected batteries," *IEEE Transactions on Aerospace and Electronic Systems*, vol. 39, no. 2, pp. 704–710, Apr. 2003.
- [7] P. Ruetschi, "Aging mechanisms and service life of lead-acid batteries," *Journal of Power Sources*, vol. 127, no. 1-2, pp. 33–44, Mar. 2004.
- [8] J. Cao, N. Schofield, and A. Emadi, "Battery balancing methods: A comprehensive review," *2008 IEEE Vehicle Power and Propulsion Conference*, pp. 1–6, Sep. 2008.
- [9] F. Altaf, L. Johannesson, and B. Egardt, "Simultaneous Thermal and State-of-Charge Balancing of Batteries: A Review," *2014 IEEE Vehicle Power and Propulsion Conference (VPPC)*, pp. 1–7, Oct. 2014.
- [10] H. Visairo and P. Kumar, "A reconfigurable battery pack for improving power conversion efficiency in portable devices," in *2008 7th International Caribbean Conference on Devices, Circuits and Systems*, Apr. 2008, pp. 1–6.
- [11] H. Sharif and M. Alahmad, "Dynamic reconfigurable multi-cell battery: A novel approach to improve battery performance," in *2012 Twenty-Seventh Annual IEEE Applied Power Electronics Conference and Exposition (APEC)*, Feb. 2012, pp. 439–442.
- [12] T. Kim, "Power Electronics-Enabled Self-X Multicell Batteries: A Design Toward Smart Batteries," *IEEE Transactions on Power Electronics*, vol. 27, no. 11, pp. 4723–4733, Nov. 2012.
- [13] M. Momayyezani, B. Hredzak, and V. Agelidis, "An Integrated Reconfigurable Converter Topology for High Voltage Battery Systems," *IEEE Transactions on Power Electronics*, vol. PP, no. 99, pp. 1–1, 2015.
- [14] W. Huang and J. a. Abu Qahouq, "Energy Sharing Control Scheme for State-of-Charge Balancing of Distributed Battery Energy Storage System," *IEEE Transactions on Industrial Electronics*, vol. 62, no. 5, pp. 2764–2776, May 2015.
- [15] N. Lotfy, R. Diefenbach, and B. Eiref, "Distributed management apparatus for battery pack," Dec. 15 1998, US Patent 5,850,351.
- [16] D. Lim and A. Anbuky, "A Distributed Industrial Battery Management Network," *IEEE Transactions on Industrial Electronics*, vol. 51, no. 6, pp. 1181–1193, Dec. 2004.
- [17] F. L. Lewis, H. Zhang, K. Hengster-Movric, and A. Das, *Cooperative Control of Multi-Agent Systems*, ser. Communications and Control Engineering. London: Springer London, 2014.
- [18] S. D. J. McArthur, E. M. Davidson, V. M. Catterson, A. L. Dimeas, N. D. Hatziaargyriou, F. Ponci, and T. Funabashi, "Multi-Agent Systems for Power Engineering Applications-Part I: Concepts, Approaches, and Technical Challenges," *IEEE Transactions on Power Systems*, vol. 22, no. 4, pp. 1743–1752, Nov. 2007.
- [19] Y. Simmhan, A. G. Kumbhare, B. Cao, and V. Prasanna, "An Analysis of Security and Privacy Issues in Smart Grid Software Architectures on Clouds," in *2011 IEEE 4th International Conference on Cloud Computing*, Jul. 2011, pp. 582–589.
- [20] Z. Yang, S. Yu, W. Lou, and C. Liu, "Privacy-Preserving Communication and Precise Reward Architecture for V2G Networks in Smart Grid," *IEEE Transactions on Smart Grid*, vol. 2, no. 4, pp. 697–706, 2011.
- [21] A. Bidram, A. Davoudi, F. L. Lewis, and J. M. Guerrero, "Distributed Cooperative Secondary Control of Microgrids Using Feedback Linearization," *IEEE Transactions on Power Systems*, vol. 28, no. 3, pp. 3462–3470, Aug. 2013.
- [22] J. W. Simpson-Porco, F. Dörfler, and F. Bullo, "Synchronization and power sharing for droop-controlled inverters in islanded microgrids," *Automatica*, vol. 49, no. 9, pp. 2603–2611, Sep. 2013.
- [23] V. Nasirian, S. Moayedi, A. Davoudi, and F. L. Lewis, "Distributed Cooperative Control of DC Microgrids," *IEEE Transactions on Power Electronics*, vol. 30, no. 4, pp. 2288–2303, Apr. 2015.
- [24] T. Morstyn, B. Hredzak, and V. G. Agelidis, "Distributed Cooperative Control of Microgrid Storage," *IEEE Transactions on Power Systems*, vol. 30, no. 5, pp. 2780–2789, Sep. 2015.
- [25] T. Morstyn, B. Hredzak, V. G. Agelidis, and G. Demetriades, "Cooperative control of DC microgrid storage for energy balancing and equal power sharing," in *2014 Australasian Universities Power Engineering Conference (AUPEC)*, no. October, Sep. 2014, pp. 1–6.
- [26] T. Morstyn, B. Hredzak, G. D. Demetriades, and V. G. Agelidis, "Unified Distributed Control for DC Microgrid Operating Modes," *IEEE Transactions on Power Systems*, pp. 1–11, 2015.

- [27] T. Morstyn, B. Hredzak, and V. G. Agelidis, "Cooperative Multi-Agent Control of Heterogeneous Storage Devices Distributed in a DC Microgrid," *IEEE Transactions on Power Systems*, pp. 1–13, 2015.
- [28] —, "Communication delay robustness for multi-agent state of charge balancing between distributed AC microgrid storage systems," in *2015 IEEE Conference on Control Applications (CCA)*, sep 2015, pp. 181–186.
- [29] C. Li, T. Dragicevic, M. G. Plaza, F. Andrade, J. C. Vasquez, and J. M. Guerrero, "Multiagent based distributed control for state-of-charge balance of distributed energy storage in DC microgrids," in *IECON 2014 - 40th Annual Conference of the IEEE Industrial Electronics Society*, oct 2014, pp. 2180–2184.
- [30] C. Li, T. Dragicevic, J. C. Vasquez, J. M. Guerrero, and E. A. A. Coelho, "Multi-agent-based distributed state of charge balancing control for distributed energy storage units in AC microgrids," in *2015 IEEE Applied Power Electronics Conference and Exposition (APEC)*, mar 2015, pp. 2967–2973.
- [31] H. Behjati, A. Davoudi, and F. Lewis, "Modular DC-DC Converters on Graphs: Cooperative Control," *IEEE Transactions on Power Electronics*, vol. 29, no. 12, pp. 6725–6741, dec 2014.
- [32] S. Moayedi, V. Nasirian, F. Lewis, and A. Davoudi, "Team-oriented load sharing in parallel dc-dc converters," *IEEE Transactions on Industry Applications*, vol. 9994, no. c, pp. 1–1, 2014.
- [33] S. Abhinav, G. Binetti, A. Davoudi, and F. L. Lewis, "Toward consensus-based balancing of smart batteries," *2014 IEEE Applied Power Electronics Conference and Exposition - APEC 2014*, pp. 2867–2873, Mar. 2014.
- [34] B. Culpin and D. Rand, "Failure modes of lead/acid batteries," *Journal of Power Sources*, vol. 36, no. 4, pp. 415–438, dec 1991.
- [35] B. Bhangu, P. Bentley, D. Stone, and C. Bingham, "Nonlinear Observers for Predicting State-of-Charge and State-of-Health of Lead-Acid Batteries for Hybrid-Electric Vehicles," *IEEE Transactions on Vehicular Technology*, vol. 54, no. 3, pp. 783–794, May 2005.
- [36] G. L. Plett, "Extended Kalman filtering for battery management systems of LiPB-based HEV battery packs," *Journal of Power Sources*, vol. 134, no. 2, pp. 262–276, Aug. 2004.
- [37] R. E. Kalman, "A New Approach to Linear Filtering and Prediction Problems," *Journal of Basic Engineering*, vol. 82, no. 1, p. 35, 1960.
- [38] M. Zhu and S. Martínez, "Discrete-time dynamic average consensus," *Automatica*, vol. 46, no. 2, pp. 322–329, Feb. 2010.
- [39] V. Blondel, J. Hendrickx, A. Olshevsky, and J. Tsitsiklis, "Convergence in Multiagent Coordination, Consensus, and Flocking," in *Proceedings of the 44th IEEE Conference on Decision and Control*, 2005, pp. 2996–3000.
- [40] J. Wang and N. Elia, "Distributed Averaging Algorithms Resilient to Communication Noise and Dropouts," *IEEE Transactions on Signal Processing*, vol. 61, no. 9, pp. 2231–2242, May 2013.



**Thomas Morstyn** (S'13) received the B.E. (Hon.) degree in electrical engineering from the University of Melbourne, Australia, in 2011.

He worked as an electrical engineer in the Rio Tinto Technology and Innovation group for two years. He is currently working towards the Ph.D. degree at the Australian Energy Research Institute, The University of New South Wales, Sydney, NSW, Australia. His current research interests include control systems for the integration of distributed renewable generation and storage into power networks.



**Milad Momayyezani** (S'15) was born in Esfahan, Iran. He received his B.Sc. degree in electrical engineering from the University of Tehran, Iran. In 2011, he started M.Sc. studies in electrical power engineering at KTH Royal Institute of Technology, Stockholm, Sweden with focus on power electronics. From 2012-2013, he moved to Germany as an exchange student and accomplished his thesis at the Institute for Power Electronics and Electrical Drives (ISEA), RWTH Aachen, Germany. He is currently pursuing his PhD studies as a member of

Australian Energy Research Institute (AERI) at the University of New South Wales (UNSW), Sydney, Australia. His current research interests include reconfigurable converters and energy storage systems.



**Branislav Hredzak** (M'98-SM'13) received the B.Sc./M.Sc. degree from the Technical University of Kosice, Slovak Republic, in 1993, and the Ph.D. degree from Napier University of Edinburgh, U.K., in 1997, all in electrical engineering.

He was a Lecturer and a Senior Researcher in Singapore from 1997 to 2007. He is currently a Senior Lecturer in the School of Electrical Engineering and Telecommunications, The University of New South Wales, Sydney, NSW, Australia. His current research interests include hybrid storage technologies and

advanced control systems for power electronics and storage systems.



**Vassilios G. Agelidis** (S'89-M'91-SM'00-F'16) was born in Serres, Greece. He received the B.Eng. degree in electrical engineering from the Democritus University of Thrace, Thrace, Greece, in 1988, the M.S. degree in applied science from Concordia University, Montreal, QC, Canada, in 1992, and the Ph.D. degree in electrical engineering from the Curtin University, Perth, WA, Australia, in 1997.

From 1993 to 1999, he was with the School of Electrical and Computer Engineering, Curtin University. In 2000, he joined the University of Glasgow,

Glasgow, U.K., as a Research Manager for the Glasgow-Strathclyde Centre for Economic Renewable Power Delivery. In addition, he has authored/co-authored several journal and conference papers as well as Power Electronic Control in Electrical Systems in 2002. From January 2005 to December 2006, he was the inaugural Chair of Power Engineering in the School of Electrical, Energy, and Process Engineering, Murdoch University, Perth. From December 2006 to June 2010, he was the Energy Australia Chair of Power Engineering at the University of Sydney. He is currently the Director of the Australian Energy Research Institute, The University of New South Wales, Sydney, NSW, Australia.

Dr. Agelidis received the Advanced Research Fellowship from the United Kingdoms Engineering and Physical Sciences Research Council in 2004. He was the Vice President Operations within the IEEE Power Electronics Society during 2006-2007. He was an Associate Editor of the IEEE POWER ELECTRONICS LETTERS from 2003 to 2005, and served as the Power Electronics Society (PELS) Chapter Development Committee Chair from 2003 to 2005. He was an AdCom Member of IEEE PELS for 2007-2009 and the Technical Chair of the 39th IEEE Annual Power Electronics Specialists Conference, Rhodes, Greece.